OFFICE OF NAVAL RESEARCH

Grant No. _____

R&T Code N00014-92-C-0173

Technical Report #09

MOLECULAR DYNAMICS COMPUTER SIMULATIONS OF CHARGED METAL ELECTRODE-AQUEOUS ELECTROLYTE INTERFACES

by

Michael R. Philpott
James N. Glosli*

Prepared for publication

in the

Proceedings of the Conference on Theoretical and Computational Approaches to Interface Phenomena
South Dakota State University
8/2/93 - 8/4/93

To be Published by
Plenham Press

IBM Research Division, Almaden Research Center,
650 Harry Road, San Jose, CA 95120-6099

1994

*Lawrence Livermore National Laboratory, Livermore, CA 94550

SECURITY CLASSIFICATION OF THIS PAGE *(When Data Entered)*

REPORT DOCUMENTATION PAGE		READ INSTRUCTIONS BEFORE COMPLETING FORM
1. REPORT NUMBER 09	2. GOVT ACCESSION NO.	3. RECIPIENT'S CATALOG NUMBER
Technical Report 16 4. TITLE *(and Subtitle)* Molecular Dynamics Computer Simulations of Charged Metal Electrode-Aqueous Electrolyte Interfaces		5. TYPE OF REPORT & PERIOD COVERED Technical Report
		6. PERFORMING ORG. REPORT NUMBER
7. AUTHOR(s) Michael R. Philpott, James N. Glosli		8. CONTRACT OR GRANT NUMBER(s) N00014-92-C-0173
9 PERFORMING ORGANIZATION NAME AND ADDRESS IBM Research Division, Almaden Research Center 650 Harry Road San Jose, CA95120-6099		10. PROGRAM ELEMENT, PROJECT, TASK AREA & WORK UNIT NUMBERS
11. CONTROLLING OFFICE NAME AND ADDRESS Office of Naval Research 800 North Qunicy Street Arlington, VA 22217		12. REPORT DATE 2/18/94
		13. NUMBER OF PAGES 26 pages
14. MONITORING AGENCY NAME & ADDRESS *(If different from Controlling Office)* Dr. Ronald A. De Marco Office of Naval Research, Chemistry Division 800 N. Quincy Street Arlington, VA 22217 U.S.A.		15. SECURITY CLASS *(of this report)* Unclassified
		15a. DECLASSIFICATION/DOWNGRADING SCHEDULE
16. DISTRIBUTION STATEMENT *(of this Report)* Approved for public release; unlimited distribution.		
17. DISTRIBUTION STATEMENT *(of the abstract entered in Block 20, if different from Report)* Approved for public release; unlimited distribution.		
18. SUPPLEMENTARY NOTES Prepared for publication in the Proceedings of the Conference on Theoretical & Computational Approaches to Interface Phenomena		
19. KEY WORDS *(Continue on reverse side if necessary and identify by block number)*		
20. ABSTRACT *(Continue on reverse side if necessary and identify by block number)* SEE NEXT PAGE		

When two different substances are joined, material flows across the interface (sometimes almost imperceptibly) until the chemical potentials of the component species are equalized. When the substances are solid or liquid and some of the chemical species are charged, then the interface develops a net electrical polarization due to the formation of an electric double layer. The main goal of this program of study is to give a molecular basis for understanding the structure and dynamics of electric double layers at charged metal-aqueous electrolyte interface. The aim is to unify current separate descriptions of surface adsorption and solution behavior and, ultimately, to include a detailed treatment of the surface crystalography and electronic properties of the metal.

MOLECULAR DYNAMICS COMPUTER SIMULATIONS OF CHARGED METAL ELECTRODE-AQUEOUS ELECTROLYTE INTERFACES

Michael R. Philpott and James N. Glosli†

IBM Almaden Research Center
650 Harry Road, San Jose CA 95120-6099
†Lawrence Livermore National Laboratory
Livermore CA 94550

INTRODUCTION

When two different substances are joined material flows across the interface (sometimes almost imperceptibly) until the chemical potentials of the component species are equalized. When the sustances are solid or liquid and some of the chemical species are charged then the interface developes a net electrical polarization due to the formation of an electric double layer. The existence of electric double layers was first recognized by von Helmholtz [1] who studied them in the last century. In many chemical and biological systems the electric double layer exerts a profound effect on function. For example in aqueous electrolyte solution the electric field of a charged object (electrode surface or an ion) is completely shielded by the movement of ions of opposite sign toward the surface until charge balance is achieved. The distribution of ions around charged objects is described simply by the classical theories of Gouy[2-4] and Chapman[5] for flat surfaces and by the theory of Debye and Hückel[6] for spherical ions.

The main goal of this program of study is to give a molecular basis for understanding the structure and dynamics of electric double layers at charged metal-aqueous electrolyte interface. The aim is to unify current separate descriptions of surface adsorption and solution behavior, and ultimately to include a detailed treatment of the surface crystalography and electronic properties of the metal. A key element in this effort is the correct treatment of electrostatic interactions among ions, polar neutrals and their images in the metal. In our work this is achieved with the use of the fast multipole method of Greengard and Rokhlin[7-10]. The fast multipole method was specifically designed for efficient computation of long range coulomb interactions. In our simulations we have used it to in the calculation of all electrical forces, including direct space and image interactions.

Because we calculate the electrostatic interactions accurately, without the use of finite cut-offs, this work also has important implications concerning the way in which ions and water distributions in biological[11] and clay suspensions[12] systems should be calculated.

Four previous publications summarize the work completed prior to that described in this report[13-16]. Through systematic computer simulations we have shown that a relatively simple model suffices to describe the adsorption of halide anions and alkali metal cations on neutral and charged metal surfaces. These calculations show qualitatively many of the features known to occur experimentally at electrochemical interfaces in the thermodynamically stable region of the electric double layer. Most notable are the existence of: highly oriented water layer next to the charged metal, contact adsorption layer of the larger ions, and a diffuse region of strongly hydrated ions. The contact adsorbed ions comprise the compact layer in electrochemical interfaces. In our model, contact adsorbed ions are physisorbed because there is no provision to describe covalent bonds. Typical electric fields found in our calculations correspond to $5x10^9$ V/m, and these arise from image charge densities on the electrode of about $0.1e/nm^2$. One by product of our simulations is to point up some of the limitations in current electrochemical concepts. Consider for example the outer Helmholtz plane which defines the position of closest approach of hydrated ions to the elctrode surface. This plane is shown in numerous textbook and review article illustrations[17, 18]. Our simulations show that the plane really corresponds to a narrow zone where ions of the diffuse layer ions penetrate with increasing difficulty the closer they are to the electrode surface. In this zone some mixing with contact adsorbed species can occur which is not possible in the old picture.

In the last fifteen years there have been many simulations of water and electrolyte solutions near surfaces. Some of these studies have contributed greatly to our understanding of electrochemical interfaces. For completeness some of this work is summarized here. Films of pure water between uncharged dielectric walls[13, 19-21], and charged dielectric walls[13, 14, 22, 23]. Some of this work is noteworthy because of a predicted phase transition[22, 23]. There have been numerous calculations reported for uncharged metal[24-27] walls[28-32], including one for jellium[30] and several for corrugated platinum surfaces[27-29, 31, 32] predicting that water adsorbs weakly at top sites with oxygen down on Pt(111) and Pt(100). There have also been some calculations for electrolyte solutions between uncharged and charged dielectric walls[13, 14, 33, 34] emphasizing spatial distributions and hydration shell structure. There have been studies for electrolytes between uncharged metal walls[27, 35, 36]. The work of Rose and Benjamin[36] is particularly interesting because umbrella sampling was used to calculate the free energy of adsorption. Finally we mention the studies of water between charged metal walls[37], and electrolytes between charged metal walls[37]. In much but not all of the work just summarized, the long range coulomb interactions were treated in an approximate way. The commonest approximation was to cut off all interactions beyond a certain radius like 0.10 nm. Some workers used the Ewald method or a planar modification of the method to compute the sum of long range fields correctly. Curiously many of the other summation methods, like the planewise method of de Wette [38] seem not to have been used at all. The reason why it is important to calculate the long range fields accurately is to capture the macroscopic part. The dipole component of the field is conditionally convergent and the sum must be performed in a manner consistent with the physical boundaries. This is a rather old problem which has a partial mapping onto the problem of calculating the macroscopic electromagnetic field inside a sample of arbitrary shape. Space and time (!) prevent us from pursuing this connection here.

CAPILLARY THERMODYNAMICS

Our present understanding of electric double layers and their importance in surface electrochemistry has its origin in the dropping mercury electrode experiments of Grahame[39, 40]. The basic experiment consists of measuring the radius of a sessile mercury drop as a function of electrode potential and electrolyte composition. One can then use the electrocapillary equations of Lippmann[41] to relate radius of the drop to the interfacial surface tension and so in turn to the charge on the electrode. Thermodynamic arguments are then used deduce the surface excess concentration of adsorbed cations, anions and neutral organics on the electrode surface[17, 18, 39, 40, 42, 43].

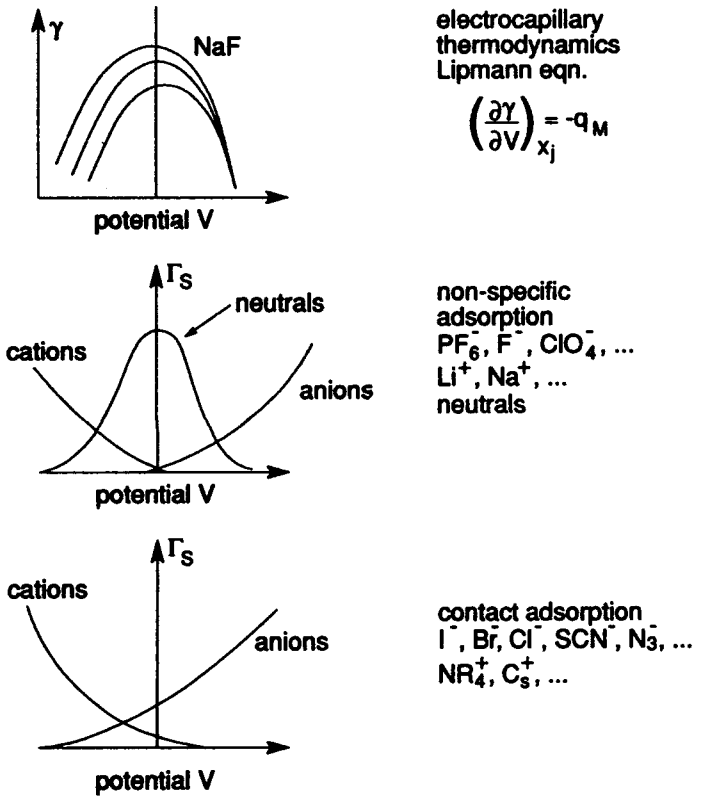

Figure 1. Schematic diagram depicting thermodynamics of adsorption: (a) plot of surface tension γ vs electrode potential V for different electrolyte compositions, (b) surface concentration Γ_S vs potential V for neutrals and strongly hydrated ions, (c) Γ_S vs potential V for contact adsorbing ions.

Figure 1 summarizes the important aspects of thermodynamic studies. For example at the top of Figure 1 the surface tension γ is depicted versus electrode potential for aqueous NaF at different concentrations. The Lippmann equation

$$\left(\frac{\partial \gamma}{\partial V}\right)_{TPN_j} = -q_M \qquad [1]$$

can be used to determine the charge on the mercury drop directly, and in turn the differential capacitance can be calculated. Contact adsorbed ions give a large contribution to the capacitance compared to ions in the diffuse layer, and this has be used to separate their

contributions in mixed solutions. The middle Figure 1 shows highly schematic curves for the adsorption of neutral organics and strongly hydrated ions on noble metals. The organics adsorb most strongly when the charge on the electrode is small because the water layer nearest the metal is then least strongly bound and more easily displaced by the organic adsorbate. The final part Figure 1c shows the adsorption isotherms for larger ions, in particular it depicts behaviour like that observed for iodide and the pseudohalides CN^- and thiocyanate SCN^-. For more discussion see the review paper by Anson[44]. For solid electrodes less direct methods are used to obtain the relevant data for a thermodynamic analysis. If the differential capacitance[45, 46]

$$C(V) = \left(\frac{\partial q_M}{\partial V} \right)_{TPN_j} \qquad [2]$$

can be measured in a way that inner layer and diffuse layer contributions can be separated then a variety of integration techniques can be used to determine the charge on the electrode. From these quantities the other important thermodynamic variables such as the surface concentrations Γ_S (depicted schematically in middle and bottom of Figure 1) can be obtained using the thermodynamic analysis starting from Eqn (1).

THE TRADITIONAL MODEL

On the basis of experimental methods like differential capacitance, chronocoulombmetry, ellipsometry, and UV-visible spectroscopy, wielded with consummate skill a detailed picture of the electric double layer adjacent to metal surfaces has been devised[18, 47]. We will refer to this picture as the 'traditional model'. The main features of this model are shown schematically in Figure 2 for that part of the double layer close to the electrode surface. Drawings similar to this one can be found in many textbooks and review articles on interfacial electrochemistry[48-50]. The metal is flat and carries charge (negative shown), the aqueous subphase is divided into two parts, called diffuse and compact regions. Additionally next to the charged surface there is a highly oriented layer of water shown in Figure 2 with protons oriented towards the surface. The anion is shown adsorbed in contact (physisorbed) and the strongly hydrated cations are shown no closer than two water molecules. The inner Helmholtz plane (IHP) is defined as the plane through the nuclei of the contact adsorbed anions and a similar plane through cations at their distance of closest approach is called the outer Helmholtz plane (OHP). Beyond the OHP the distribution of ions is assumed to be described by the Gouy-Chapman theory, which in it's simplest form assumes the ions are charged point-like objects and the solvent is a dielectric continuum with appropriate bulk properties. Close to the electrode the 'traditional model' calculates system properties based on static distributions or uses lattice statistics. The diffuse region in this picture[18] starts two solvent molecules from a flat electrode surface and stretches out several nanometers into the bulk electrolyte. The electrostatics and ionic distributions in this diffuse part were first described by the Gouy-Chapman theory[2-5] which predates even the Debye-Hückel[6] model of ionic atmospheres in bulk electrolytes. The ions in the diffuse layer screen the net charge of metal and any ions occupying in the compact part of the double layer. Traditionally the structure of the compact region is thought of as being rather static and resembling a parallel plate capacitor with a gap of atomic separations (0.1 - 0.2 nm). The flat surface model dates from times before the ability to make useable single crystal electrode surfaces, the advent of synchrotron sources and facilities to do surface X-ray analysis. Even so quite a consid-

erable effort has been directed toward developing better model of the metal side. In this regard the work of Halley et al[51-53] and Schmickler[54] is particularly significant. These groups have developed theories based on jellium electrode models of the charged metal surface that attempts to capture important physics causing features in measured capacitance vs. potential curves. Focussing more on the electrolyte subphase Henderson and coworkers[55] have developed a correlation function approach and an analysis that shows that in their very reasonable model there is no sharp division between the diffuse and inner Helmholtz planes. This is in contrast to the ideas conveyed by the pictures found in many textbooks and Figure 2.

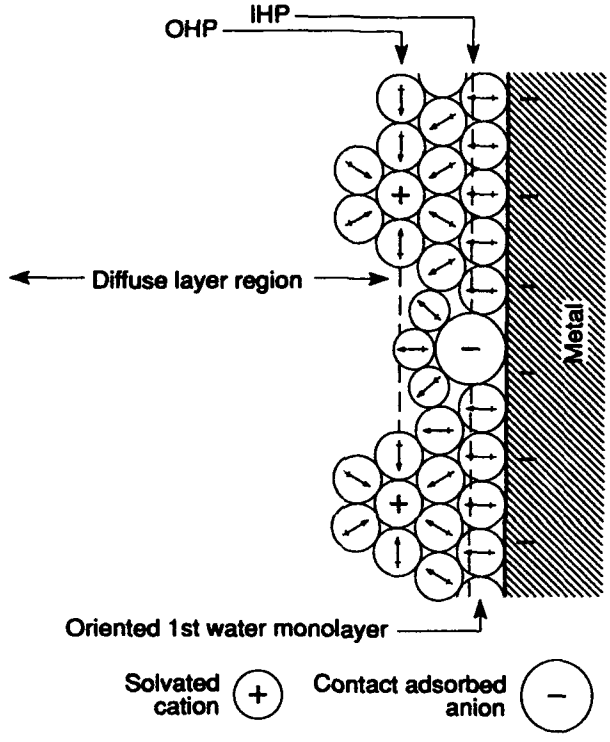

Figure 2. Schematic diagram depicting the 'traditional model' of the electric double layer found in many review articles and introductory texts on electrochemistry.

It must be pointed out that many of molecular dynamics studies performed to date have not recognized the importance of solving the electrostatics problem accurately. Intense long range fields exist at the interface because of the large dipole normal to the surface formed by the ions and their electrical images are all in phase. This problem spills over into other areas where electrostatics is important, for example most studies of water around biological objects are wrong in the way in which the dielectric polarization of water is calculated because long range correlations are lost when interactions are cut off at a finite distance. Workers in this field often resort to using distance dependent dielectric functions to shield ionized groups attached to the object's surface.

The experimental picture of electrochemical surfaces is currently undergoing rapid change due to numerous advanced in situ and ex situ UHV surface science probes of the electrochemical interface. The new synchrotron based X-ray surface crystal structure probes like grazing incidence X-ray scattering (GIXS), X-ray standing wave (XSW), surface extended X-ray absorption fine structure (SEXAFS) techniques have allowed surface geometries to be measured for the first time[56-59]. Recent studies by Hubbard and

coworkers[46] reveal changes in charge state of the ion as the surface concentration is increased, changes that have analogies in UHV surface science studies of the metalization of semiconductors These studies show contact adsorption to be a complex process that can evolve into chemisorption at high coverages even if the initial step is physisorption. Local probes like scanning tunneling microscopy (STM) and atomic force microscopy (AFM) give images with local atomic scale features. The next few years will likely see major revisions in our experimental understanding of the less dynamic part of the electrochemical double layers.

MODEL FOR THE IMMERSED ELECTRODE

Consider a system consisting of two electrodes immersed in aqueous electrolyte solution as shown schematically in Figure 3. Reading from left to right there are three regions: the anode on the left, the bulk region at the center, and the cathode region on the right. If the electrodes are uncharged then in all three regions the electrolyte phase would be electrically neutral. Now when the externally applied (battery) potential is altered so that the electrodes become charged (the case shown schematically in Figure 3) the electrolyte responses by screening the electric field and the three regions acquire different net charge. One with excess anions (left) screens the positive charge on the left electrode, a bulk region in which the electric field is zero, and one with an excess of cations (right). When the charge on each electrode is included with the adjacent 'zone' of electrolyte the net charge in each region is zero.

These simple considerations suggest we can try to model an immersed electrode with it's adjacent screening region and do not have to model the whole cell as was done in two previous publications[13, 14]. This approach is useful because it reduces the number of water molecules in the calculation, however it imposes a constraint in the form of charge neutrality and requires us to choose a 'good' boundary to separate the bulk region and immersed region. We can test the boundary by scaling the size of the system to capture some bulk-like behavior. Scaling by a factor of ten suggests that four layers of water is a minimum sized system.

Our immersed electrode model therefore consists of a layer of electrolyte between two walls. The wall on the left carries no charge it is simply a restraining wall and ideally should allow a continuous transition to the bulk electrolyte region. The complete system of electroltye and electrode (always chosen to be on the right hand side in our calculations) is neutral, unless we deliberately choose to stress the system with an uncompensated charge on the right hand metal electrode. In practice we have performed both types of calculation for reasons described in more detail later. Later we will show an important result that water behaves in an uncompensated field as if the excess ionic charge were higher.

Since there is integer charge in the aqueous phase q_{Aq}, and the image charge on the metal q_{im} satisfies the equation $q_{im} + q_{aq} = 0$. In our calculations we also consider cases (to be discussed at length later) where there is additional charge q_{uc} on the electrode with the restriction that $q_T = q_{im} + q_{uc} = ne$ where $n = 0, \pm 1, \pm 2, \ldots$.

In Figure 3 if one thinks of the vertical dash line as symbolizing the restraining wall then in reality the vertical line will be very close to the corresponding electrode for a macroscopic sized cell. Integral electrode charge is an essential constraint in this immersed electrode model. We stress again that the main advantage of the model is that

only about half the number of water molecules are needed to simulate a system with two metal electrodes. For the restraining barrier we choose a 9-3 potential. The origin for this restraining potential is at 1.862 nm from the image plane of the metal. We refer to this restraining potential surface as the dielectric surface, and as already mentioned it's only function is to limit the extent of the fluid phase and thereby make the calculations more tractable. In all the calculations reported here the simulation cell was a cube with edge 1.862nm. The cube was periodically replicated in the xy directions parallel to the electrode surface plane. Again we mention that we have performed some scaled up calculations on cells with larger edge length by up to a factor 2 and found very similar features to those described for the smaller cells.

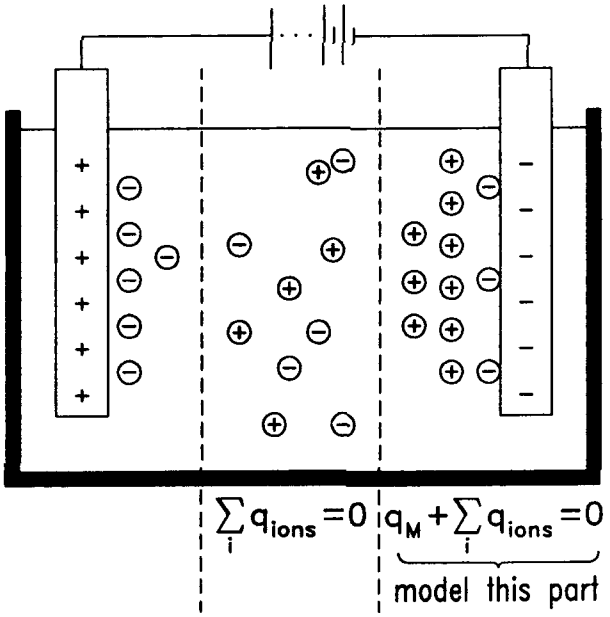

Figure 3. Immersed Electrode Model. Schematic diagram of the electrochemical cell showing the immersed electrode configuration on the right side. Vertical broken lines symbolize the transition region from diffuse layer to bulk electrolyte where the solution is electrically neutral.

MODEL FOR WATER, IONS AND THE METAL SURFACE

In all the calculations reported here we have used the parameters of the Stillinger[60, 61] ST2 water model and the extensive interaction parameter set for alkali metal ions and halide ions developed by Heinzinger and coworkers[62]. Figure 4 shows a schematic of the ST2 water model, a simple ion and the smoothly truncated Lennard-Jones potential. The ST2 water molecule model consists of a central oxygen atom (O_ST2 or O for short) surrounded by two hydrogen atoms (H_ST2 or H for short) and two massless point charges (PC_ST2 or PC for short) in a rigid tetrahedral arrangement (bond angle = $\cos^{-1}(1/\sqrt{3})$). The O-H and O-PC bond lengths were 0.10 nm and 0.08 nm respectively. This small difference in bond lengths means that the water_ST2 model and its electrostatic image (i.e., $q \rightarrow -q$) behave similarly. The only Lennard-Jones 'atom' in ST2 model is the oxygen atom. The hydrogen H and point charges PC interact with their surroundings (i.e., other atoms and surfaces) by Coulomb interactions only. Their charges are q_H= 0.23570|e| and q_{PC}= $-q_H$. The O atom carries no charge. The alkali metal ion and halide ion were treated as non-polarizable Lennard-Jones atoms with central point mass and

charge. Figure 4 shows an ion schematically next to the water model. The atom-atom interaction parameters are taken from Heinzinger's review[28, 62].

Next we describe the interaction between water and ions and the metal and restraining wall. The metal was represented by two linearly superimposed potentials. Pauli repulsion and dispersive attractive interactions were modelled by a 9-3 potential, and the interaction of charges with the conduction electrons by a classical image potential. In the calculations described here the image plane and origin plane of the 9-3 potential were coincident. This was tantamount to choosing the image plane and the nuclear plane of the metal surface to be coincident. This was acceptable in our scheme because the Lennard-Jones core parameters σ are all large and the 'thickness' of the repulsive wall is also large (ca. 0.247 nm).

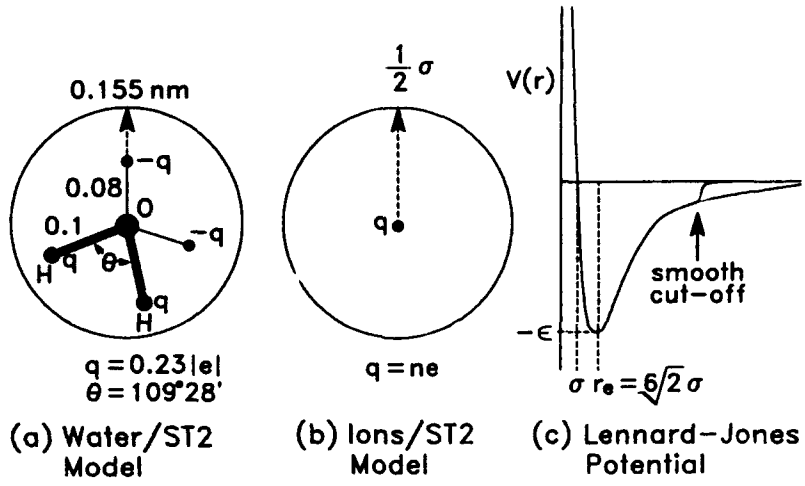

Figure 4. The Ion and Water Models. Schematic diagram summarizing the key features of the model for ST2 water and the ions. Water and ions are treated as non polarizable Lennard-Jones atoms with embedded charges. Shown on the left is a schematic drawing of the Lennard-Jones potential with smooth cut-off.

CALCULATION OF THE ELECTROSTATIC INTERACTIONS

Electrostatic sums are conditionally convergent and great care must be exercised in using cut-offs and different boundary conditions. The Coulomb field computation grows as N^2 (N number of charged particles) unless special measures are adopted. We use the fast multipole method (fmm) devised by Greengard and Roklin[7], in which the cpu time grows as N. The cross over point in efficiency for direct sum versus fmm can be as small as N = 1000 (about 250 ST2 water molecules). The original papers of Greengard should be consulted for details of this clever algorithm. Some discussion of the use of fmm in electrochemical simulations has been given by Glosli and Philpott[15].

TOTAL POTENTIAL ENERGY OF THE SYSTEM

The Coulomb interaction between molecules was represented as sum of $1/r$ interactions between atomic point charges. For the ST2 water model these interactions result in H-bonds that are too strong when the PC and H atoms are close. These interactions were softened for small molecular separation in the way described by Stillinger[60] and Lee et

al[19] by introducing a switching function S that modifies specified atomic coulomb interactions at small separations. The short range part of the intermolecular interaction was modeled by Lennard-Jones potential between atom pairs on each molecule. All molecule-molecule Lennard-Jones type interactions were cut-off in a smooth fashion at a molecular separation $R = 0.68$ nm by a truncation function T. The atoms of each molecule also interacted with the surfaces at $z = \pm z_o$ where z_o = 0.931 nm. Both surfaces were treated as flat featureless plates with a uniform electric charge density of σ on the metal plate at $+z_o$ if there is an uncompensated charge on the metal, otherwise $\sigma = 0$ This gave rise to a uniform electric field, $E = 4\pi K\sigma$, in the z-direction where K the electrostatic coupling constant had the value 138.936 kJ.nm/(mole.e^2) in the units of this paper. The complete interaction energy U was given by the following formula

$$U = \sum_{\substack{\beta\in A_j \\ i<j}} \left(\left\{ \frac{Kq_\alpha q_\beta}{r_{\alpha\beta}} \left[S(R_{ij}, R_L^{ij}, R_U^{ij}) - 1 \right] + 4\varepsilon_{\alpha\beta} \left[\left(\frac{\sigma_{c\beta}}{r_{\alpha\beta}} \right)^{12} - \left(\frac{\sigma_{\alpha\beta}}{r_{\alpha\beta}} \right)^{6} \right] \right\} T(R_{ij}) + \frac{Kq_\alpha q_\beta}{r_{\alpha\beta}} \right) \qquad [3]$$

$$+ \sum_\alpha \left\{ -q_\alpha E z_\alpha + \left(\frac{A_\alpha}{(z_\alpha + z_o)^9} - \frac{B_\alpha}{(z_\alpha + z_o)^3} \right) + \left(\frac{A_\alpha}{(z_\alpha - z_o)^9} - \frac{B_\alpha}{(z_\alpha - z_o)^3} \right) \right\}$$

where i and j were molecular indices, and α and β were atomic indices. The symbol A_i represented the set of all atoms of molecular i . The symbol R_{ij} was the distance between the center of mass of molecules i and j. The symbol $r_{\alpha\beta}$ was the distance between atoms α and β. For small R we followed the practice of modifying the the coulomb energy between ST2 molecules and ions by the switching function $S(R, R_L, R_U)$ given by,

$$S(R, R_L, R_U) = \begin{cases} 0 & R < R_L \\ \dfrac{(R - R_L)^2 (3R_U - 2R - R_L)}{(R_U - R_L)^3} & R_L < R < R_U \\ 1 & R_U < R \end{cases} \qquad [4]$$

The values of R_L and R_U were dependent on the types of the molecular species that were interacting. As mentioned above the tails of the Lennard-Jones pair interactions were cut off by the truncation function T. The form of T was given by,

$$T(R) = \begin{cases} 1 & R < R_L^T \\ \left(1 - \left(\dfrac{R - R_L^T}{R_U^T - R_L^T} \right)^m \right)^n & R_L^T < R < R_U^T \\ 0 & R_U^T < R \end{cases} \qquad [5]$$

The same truncation function has been applied to all non Coulombic molecular interactions, with R_L^T=0.63 nm and R_U^T=0.68 nm. The integers m and n controlled the smoothness of the truncation function at R_L^T and R_U^T respectively. In this calculation $n = m = 2$ which insured that energy has continous first spatial derivatives.

All the atom-atom and atom-surface interaction parameters are given in Table I. For example we see that the (ε,σ) pairs are (0.3164, 0.3100), (0.1490, 0.2370) and (0.4080, 0.5400) for O_ST2, Li ion and I ion respectively. The units of the well depth ε are kJ/mole and the van der Waals σ is in nm . The usual combining rules were enforced for unlike species, namely: $\varepsilon_{AB} = (\varepsilon_{AA}\varepsilon_{BB})^{1/2}$ and $\sigma_{AB} = \frac{1}{2}(\sigma_{AA} + \sigma_{BB})$. The st2 model switching

function (see later) interval ends R_L^{IJ} and R_U^{IJ} both vanish except for st2/st2 water pairs, where $R_L^{ST2,ST2}$=0.20160 nm and $R_U^{ST2,ST2}$=0.31287 nm.

The atom-surface parameters describing interaction with nonconduction electrons were chosen to be the same as those used by Lee at al[19], A=17.447x10^{-6} kJ(nm)^6/mole and B=76.144x10^{-3} kJ(nm)^3/mole for O, I ion and Li ion. The A and B parameters for H_st2 and PC_st2 were set to zero. The potential corresponding to these parameters describe a graphite-like surface. Real metals would have much larger ε ours were deliberately chosen to be small so as to permit coulombic interactions to dominate the physics.

Table I. The interaction parameters (q, ε, σ, A, B) and mass (m) for all atoms used in the simulations, where $q_o = e$, $\varepsilon_o = 1 KJ/mole$, $\sigma_o = 1nm$, $A_o = 17.447 \times 10^{-6} KJ \cdot nm^6/mole$, $B_o = 76.144 \times 10^{-3} KJ \cdot nm^3/mole$, and $m_o = 1 AMU$. The ε and σ for unlike atom pairs are formed using the combination rules $\varepsilon_{AB} = \sqrt{(\varepsilon_{AA}\varepsilon_{BB})}$ and $\sigma_{AB} = (\sigma_{AA} + \sigma_{BB})/2$.

	q/q_o	$\varepsilon/\varepsilon_o$	σ/σ_o	m/m_o	A/A_o	B/B_o
O_ST2	0.0000	0.316	0.310	16.0	1	1
H_ST2	0.2357	0.000	0.000	1.000	0	0
PC_ST2	– 0.2357	0.000	0.0	0.0	0	0
Li	1.0000	0.149	0.237	6.9	1	1
F	– 1.0000	0.050	0.400	19.0	1	1
Cl	– 1.0000	0.168	0.486	35.5	1	1
Br	– 1.0000	0.270	0.504	79.9	1	1
I	– 1.0000	0.408	0.540	129.9	1	1

In the equations of motion bond lengths and angles were explicitly constrained by a quaternion formulation of the rigid body equations of motion[63]. The equations of motion were expressed as a set of first order differential equations and a fourth order multi-step numerical scheme with a 2 fs time step was used in the integration. At each time step a small scaling correction was made to the quaternions and velocities to correct for global drift. Also the global center of mass velocities in the x and y directions was set to zero at each time step by shifting the molecular translational velocities.

In the analysis of configurations the first 100 ps were used to equilibrate the system and subsequent configurations were used in compute properties like density profiles. There were exceptions where it was evident that the system had not equilibrated. In practice it was found this occurred frequently in three ion systems, as in the case of a cation in the presence of two coadsorbed iodide ions. All the simulations were run to 1000 ps or longer, so that generally 900 or more configurations one ps apart were used to calculate averages. Typical density plots were derived from bining configurations stored every ps and with bin widths of 0.005 nm or larger.

EQUATIONS OF MOTION

All molecules, in this study, were assumed to be a rigid collection of point atoms, so that all bond lengths and bond angles within a molecule were fixed. To evolve a collection of these molecules a quaternion formulation of the rigid body equations of motion was used[63-65] The center of mass position ($\mathbf{R}_i$) and velocity ($\mathbf{V}_i$) was used to describe the translational degrees of freedoms of molecule *i*. The orientational motion of the molecule was described by the quaternion $\mathbf{q}_i = (q_i^0, q_i^1, q_i^2, q_i^3)$ and the rotational velocity (ω_i^b), as measured in the body frame of the molecule. The one exception to this was for monatomic molecules, in which case the orientational degrees of freedom were not needed.

The discussion of the equations of motion begin by considering the potential energy U. From Eqn 3, it can be seen that the potential energy can be treated as a scalar function of the variables ($\mathbf{R}_1,..., \mathbf{R}_N; \mathbf{r}_1,..., \mathbf{r}_n$), where N is the number of molecules and n is the number of atoms in the entire system.

$$U = U(\mathbf{R}_1,..., \mathbf{R}_N; \mathbf{r}_1,..., \mathbf{r}_n) \qquad [6]$$

Of course not all these variables are independent. However for the purposes of the following two definitions they are treated as independent variables.

$$\mathbf{f}_\alpha \equiv -\nabla_{\mathbf{r}_\alpha} U, \qquad \mathbf{F}_i \equiv -\nabla_{\mathbf{R}_i} U. \qquad [7]$$

The total force $\mathbf{F}_i^T$ and torque τ_i, can be expressed in terms of $\mathbf{f}_\alpha$ and $\mathbf{F}_i$ as

$$\mathbf{F}_i^T = \mathbf{F}_i + \sum_{\alpha \in A_i} \mathbf{f}_\alpha \qquad \tau_i = \sum_{\alpha \in A_i} (\mathbf{r}_\alpha - \mathbf{R}_i) \times \mathbf{f}_\alpha, \qquad [8]$$

The translational motion of the molecule is described by the first order ordinary differential equation,

$$\frac{d\mathbf{R}_i}{dt} = \mathbf{V}_i \qquad M_i \frac{d\mathbf{V}_i}{dt} = \mathbf{F}_i^T. \qquad [9]$$

For the rotational motion it is convenient to work in the body axis of the molecule, where the moment of inertia $\hat{I}_i$ is diagonal and time independent. It is useful to define the operator $\hat{Q}_i$

$$\hat{Q}_i = \begin{bmatrix} -q_i^1 & -q_i^2 & -q_i^3 \\ q_i^0 & -q_i^3 & q_i^2 \\ q_i^3 & q_i^0 & -q_i^1 \\ -q_i^2 & q_i^1 & q_i^0 \end{bmatrix} \qquad [10]$$

and the body frame rotational force

$$\mathbf{F}_i^R = \tau_i^b - \omega_i^b \times (\hat{I}_i^b \omega_i^b). \qquad [11]$$

Using these quantities above, the following first order ordinary differential equations can be written to describe the rotational motion

$$\frac{d\mathbf{q}_i}{dt} = \hat{Q}_i \omega_i^b \qquad \hat{I}_i^b \frac{d\omega_i^b}{dt} = \mathbf{F}_i^R. \qquad [12]$$

This set of equations conserve the total energy for time independent potentials (U) . A constant temperature ensemble may be simulated by introducing a velocity dependent term in the acceleration terms to constrain the total kinetic energy. The constant temperature equations of motion are written as

$$\frac{d\mathbf{R}_i}{dt} = \mathbf{V}_i, \qquad M_i \frac{d\mathbf{V}_i}{dt} = \mathbf{F}_i^T - \gamma \mathbf{V}_i$$

$$\frac{d\mathbf{q}_i}{dt} = \hat{Q}_i \omega_i^b, \qquad (\hat{I}_i)^b \frac{d\omega_i^b}{dt} = \mathbf{F}_i^R - \gamma \omega_i^b, \qquad [13]$$

$$\gamma = (\sum_i \mathbf{V}_i \mathbf{F}_i^T + \omega_i^b \mathbf{F}_i^b)/(2K)$$

This choice of γ ensures that the total kinetic energy of the systems is constant.

INTRODUCTION TO THE RESULTS

The purpose of this section is to briefly introduce and explain some of the terms and concepts used in the description and discussion of the results. We define inner layer, inner surface field and the external or as we will also refer to it the 'uncompensated' field.

In our calculations the inner layer is defined to be all ions and molecules in contact with the electrode. Recall that the surface is represented by a 9-3 potential that acts on the center of the molecules and ions. This means that in our model the inner most layer, i.e., the first layer, has a simpler structure because steric effects due to dimension perpendicular to the surface are suppressed. In a more realistic model Pauli repulsion would ensure that the center of water was closer to the surface that the center of an iodide ion. One consequence of our model is that some hydrophobic effects at the surface are accentuated, and some steric effects based on volume are decreased in importance.

In equilibrium states the charge on the flat electrode is just the net image charge, which is equal in magnitude but opposite in sign to the sum of the charges on the ions. In this case there is no field in the bulk because the fields from the ions and their images cancel. When the charge on the electrode is only the image charge, then the potential drop occurs

between the metal surface and the ions. There is essentially no electric field beyond the ions. We call the field generated by the ions and their images the inner surface field. Since the water molecules have large permanent dipole moments those molecules between the ions and the metal will try to align with the field.

It is useful from the theoretical point of view to stress the system by placing extra uncompensated charge on the electrode. In this case there is a field across the sample, just as occurs when we have water without ions between charged plates. We refer to this field as the external, applied or uncompensated electric field. In general then we can think of the total charge on the electrode as the sum of the image charge and the extra uncompensated charge. In passing we emphasize again that in electrochemical systems it is not possible to have uncompensated charge (i.e., unshielded) on an electrode immersed in electrolyte. However, it is possible in principle to place uncompensated charge on an emersed electrode, so that there are physically realizable states resembling those of the immersed model with uncompensated charge. However the uncompensated charge densities reachable in practice are about 100 times smaller than the ones used in this paper. In our calculations with uncompensated charge we have deliberately chosen charge densities equal in magnitude to the image charge density in order to better understand the effect of the surface field on the inner layer of water.

Finally we state again that the inner surface field is localized close to the metal, in contrast to the field of uncompensated charge which extends across the entire sample. At the surface the total surface field consists of the inner field and any applied field due to uncompensated charge.

POSITIVELY CHARGED METAL IN WATER WITHOUT IONS

Water is the common primary chemical species in all the calculations described in this paper and it is important to know its behaviour in electric fields without the additional structure changing effects of ions. In this simulation 158 ST2 model water molecules were confined between the metal surface at $z_0 = 0.931$ nm and the 'dielectric' wall at $z = -z_0$. Gap between surfaces is $\Delta z = 1.862$ nm = L the edge length of the simulation cell. The water film thickness corresponds to about 4.5 layers of water. For comparison we note that in the calculations of Lee, McCammon and Rossky[19] there were 216 water ST2 molecules equivalent to about six layers. The image plane of the metal was at z = 0.931 nm the right hand surface. Left confining boundary is a dielectric surface (with dielectric constant ε=1) with no image field. The repulsive part of the 9-3 potentials on both sides of the box began at |z|=0.682 nm.

There are no ions in this sample. The electric field across the system comes from (uncompensated) positive charge density of $q_T = q_{uc} = +1$ on plate with area L^2, or equiv-

alently an charge density of $0.29e/(nm)^2$. The electric field in vacuum due to this charge is about 5.2 GV/m . Density profiles in the z direction were obtained by averaging 900 configurations over the xy plane. These profiles are shown in Figure 5. The total surface field is just the applied field. Since the field attracts negative charge to the metal the water orients with point charges PC_ST2 directed towards the metal. In comparing Figure 5 profiles with similar ones obtained by reversing the direction of the external field (not shown here) we note there is slightly more structure in the negative field than in zero field (not shown here) or the positive field (Figure 5). The structure is most prominent on the metal side because the O-H bond is longer than PC-O bond and so the proton-proton image interaction being larger pulls the water molecule closer to the metal.

In the PC_ST2 density profile in Figure 5 a distinct shoulder occurs at about 0.7 nm clearly inside the repulsive region of the 9-3 potential. This is permitted because the wall potential acts the center of the water molecule not the component atoms. That the system is strongly polarized as shown by the z component of the dipole density $\rho_p(z)$., and the microscopic charge density $\rho_q(z)$. There is a very pronounced oscillation at the surface in both profiles. Given the existence of oscillations in $\rho_{wat}(z)$ these are not unexpected. What is not clear is whether they result from the superposition of two wall effects. This has been checked with larger N simulations where they occur to the same degree implying the oscillation is intrinsic to one surface. The microscopic charge density has a small value in the interior region of the film and a large oscillation centered at approximately 0.7 nm. The dipole polarization shows large negative deviations at both surfaces, and a uniform positive value across the interior. The behaviour of the dipole and charge densities is that consistent with a high dielectric response material.

All the simple rigid water models display dielectric saturation at high fields because reorientation is the possible relaxation process, and when the molecules are all highly oriented the dielectric is saturated. In the fields in the calculations used by Brodsky et al[22, 23] water was highly oriented and close to saturation, since their system like the one studied here polarizes by molecular reorientation. We have also repeated our calculations in fields up to 1.5 times stronger and find that the interior polarization increases linearly, implying that dielectric saturation has not occurred. However the response of molecules near the surface is different and the dipolar density did not increase linearly with the external field. This is consistent with the presence of more highly oriented and more densely packed water molecules next to the surfaces.

The question of dielectric response of thin films and near surfaces in larger systems is of great interest. If we assume linear response of the electric polarization to an external field then the dielectric constant is given by

$$\frac{\varepsilon_0}{\bar{\varepsilon}} = 1 - \frac{1}{2zq_T}\int_{-z}^{z} \bar{P}_z(z')\,dz' \qquad [14]$$

In the integrand $\bar{P}_z$ is the dipole density parallel to the surface normal (z) averaged over the xy plane. The electrode charge is q_T, and the integration limit is bounded $z < L/2$. The central portion of the dipole density is linear in the applied field, and appears to provide a convenient 'quick' and unambiguous way to calculate the dielectric 'constant' $\bar{\varepsilon}_{zz}$. However in practise this is not easily realized because to check convergence one must evaluate the integral for very large system to avoid interference from the walls.

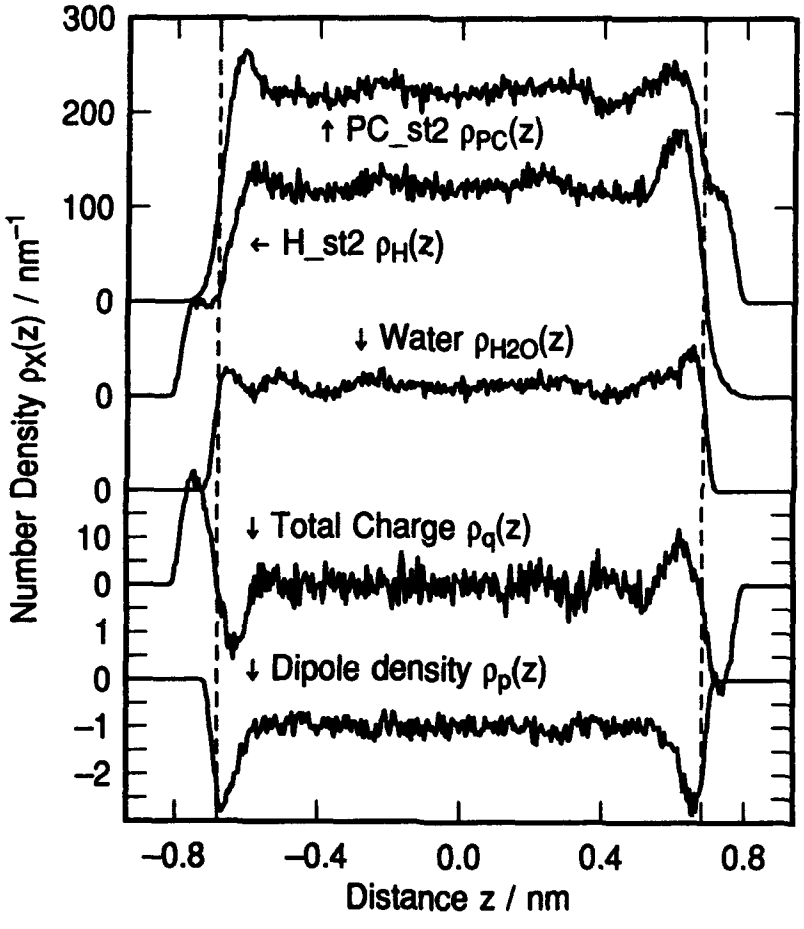

Figure 5. Water without any ions between charged plates with $q_T = q_{wc} = +1$. Component density profile plots for 158 ST2 water molecules adjacent to charged metal electrode on right side. The total electric charge density on the electrode is one positive electron on the simulation plate of area L^2, where L = 1.862 nm. 0.29 e/(nm)^2 The vacuum electric field is approximately 5 GV/m.

FLUORIDE SOLUTIONS. STRONG ELECTRIC FIELD EFFECTS.

In this section we discuss several simulations performed with one and two fluorides in the cell (effective ionic concentrations of 0.35 M and 0.70 M respectively) containing 157 and 156 water molecules respectively. We will show that at the higher concentration there is

more dense oriented layer of surface water and that the inner surface electric field drives the effect.

Figure 6 shows some representative results for one fluoride ion in the form of density profiles for the fluoride ion and the atomic components of water. In this calculation $q_T = q_{im} = +1$ and $q_{uc} = 0$. The surface field arises from the negatively charged fluoride ion and its image. Because the ion is distributed uniformly in the xy plane the surface electric field is similar to that inside a capacitor (with a 1.4 nm gap). Features in the water density profiles near the metal surface resemble those already seen for water without ions in Figure 5.

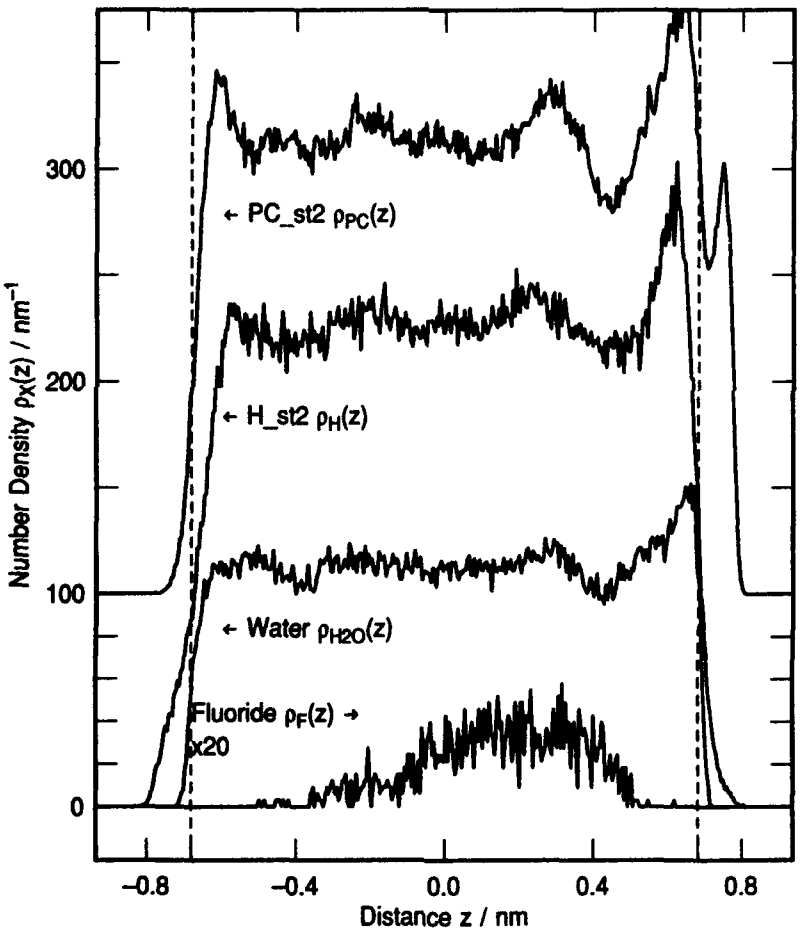

Figure 6. Adsorption of fluoride anions. Density profiles for one fluoride F^- and 157 ST2 water molecules between a metal electrode and the dielectric boundary. Charge on the metal $q_T = q_{im} = +1$. Image plane at z = 0.931 nm . Repulsive portion of the wall potentials begin at |z| = 0.682 nm. Note oriented water layer forming near the metal (rhs) with point charge (PC top curve) pointing at metal.

Features on the left at the dielectric boundary do not compare well, in fact they resemble water in zero field (not shown here). These results show that in the single ion case there is no field at the dielectric and a high field at the metal surface. This indicates that the

inner field felt by surface waters is similar to the externally applied field in the absence of ions. Closer comparison shows that at the metal side the water peaks are uniformly stronger. In particular the PC_ST2 density profile shows a distinct peak near 0.75 nm, to be compared with the shoulder at 0.7 nm in Figure 5. The extra height and structure may be due to water in the solvation sheath of the fluoride ion at its position of closest approach. Recall that the fluoride ion is strongly hydrated and shows no propensity to contact adsorb. Fluoride remains hydrated even at the point of closest approach (ca. 0.55 nm) to the metal. However at this distance the solvation shell is splayed against the electrode. The distribution is broad (-0.4 nm to 0.5 nm, peak near 0.2 nm) covering almost all accessible configuration space consistent with the ion being strongly hydrated and a permanent resident of the diffuse layer. Note also that the fluoride distribution is diffuse across the entire water film, and there being no hint of a sharp plane or barrier (equivalent to an outer Helmholtz plane OHP in the traditional model) across which the ion is prevented from passing. In these simulations the fluoride behaves more like a strongly hydrated ion in the Grahame model of the electric double layer. Figure 7 shows density profiles for the case of two fluoride ions in the simulation cell with 156 water molecules. The total microscopic charge density is also shown. Charge on the metal $q_T = q_{im} = +2$. The density profile for two fluorides resembles that of a single fluoride except it is shifted further from the metal (range is from -0.5 to 0.5 nm with the peak near 0.0 nm). The *electric field due to metal charge and ions is zero near* the dielectric boundary as seen by comparing water component profiles with previous two figures. The inner surface field has a much higher value as judged by sharper more intense peaks near the metal surface. The sharp water peak near 0.65 nm has twice the interior density value. Some of this water has one PC pointing at the electrode. Also note that the fluoride density profile is shifted away from the metal surface, consistent with the notion that the compacted layer of surface water hinders the approach of strongly hydrated ions. This effect is consistent with the concept of the OHP being approximately two water molecules distant from the electrode. The position of the first H_ST2 peak, and the near surface oscillation in microscopic charge confirm the overall picture as described.

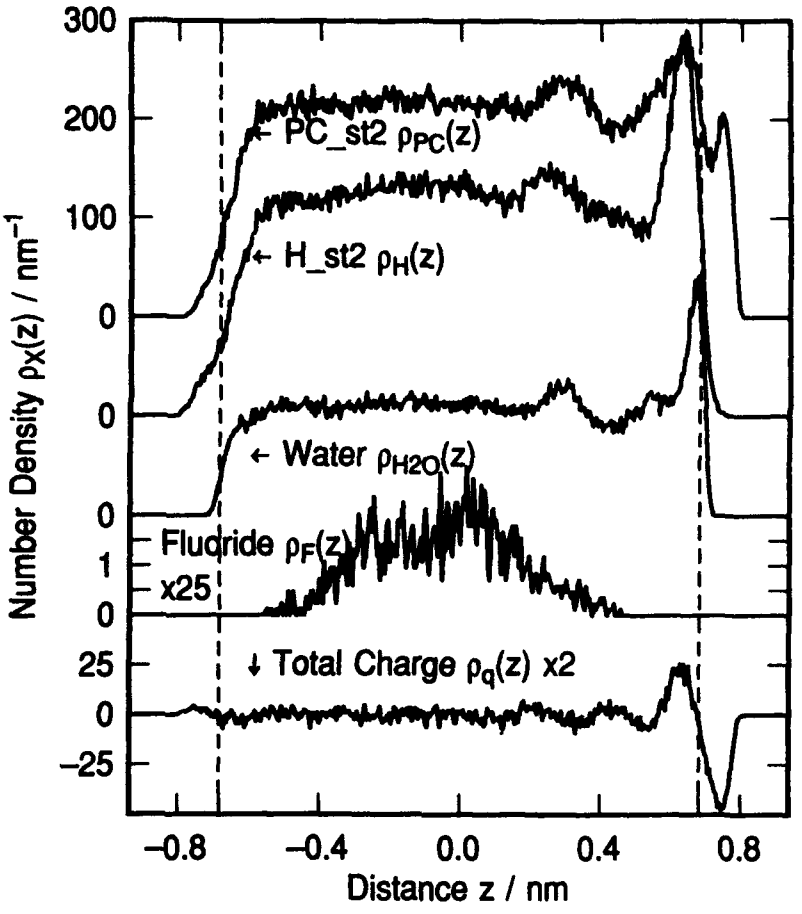

Figure 7. Adsorption of anions continued. Density profiles for two fluoride F^- and 156 ST2 water molecules between a metal electrode and the dielectric boundary. Charge on the metal $q_T = q_{im} = +2$. Image plane at z = 0.931 nm. Repulsive portion of the wall potentials begin at |z| = 0.682 nm. Note the high density oriented water peak near 0.65 nm and the shift in the fluoride distribution away from the metal compared to Figure 6.

Next we show the importance of the long range interfacial dipole field by repeating the calculation for one fluoride shown in Figure 6 with an uncompensated field equivalent to a charge of one positive electron on the plate area L^2. The charge on the metal is given by $q_T = q_{im} + q_{uc} = +2$, with $q_{im} = q_{uc} = +1$. Figure 8 shows the density profiles for one fluoride F^- and 157 ST2 water molecules between a charged metal electrode and a dielectric boundary. Note the similarities in the density profiles for water and its components in the range z > 0 nm in Figures 7 and 8. In this region the density profile almost superimpose. Since we have shown that the water profiles are sensitive to the electric field it suggests that the inner fields are almost the same in the two cases. Furthermore these calculations show that it is the field in the inner layer and not steric effects due to ions that drives the structural changes.

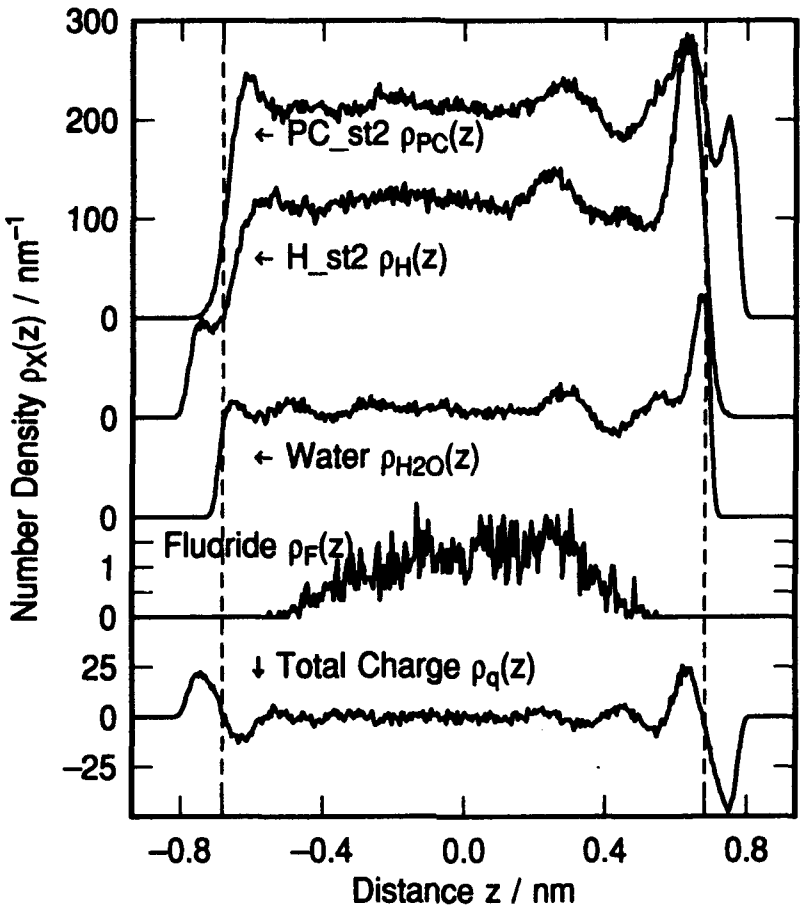

Figure 8. Adsorption of anions continued. Surface electric field effects. The charge on the metal is given by $q_T = q_{im} + q_{uc} = +2$, with $q_{im} = q_{uc} = +1$. Density profiles for one fluoride F^- and 157 ST2 water molecules between a charged metal electrode and a dielectric boundary. Note similarity of water and component density profiles in Figure 7 for z > 0 nm. Image plane at z = 0.931 nm. Repulsive portion of the wall potentials begin at |z| = 0.682 nm.

ELECTRIC FIELD EFFECTS. CASE STUDY OF SODIUM FLUORIDE

In this section we consider the effect of interchanging anions and cations with similar strengths of hydration. We have chosen NaF solutions to explore this case, and have chosen to work also with an uncompensated field ($q_{uc} = \pm 1$) to mimic higher effective concentrations than actually used in the calculation.

Figure 9 shows the density profiles for a simulation with one fluoride F^-, two sodium ions Na^+ and 155 ST2 water molecules between a charged metal electrode and a dielectric boundary. The charge on the metal was $q_T = q_{im} + q_{uc} = -2$, with $q_{im} = q_{uc} = -1$. Note that even though the field has opposite sign there is a superficial similarity of water density profile with those shown in Figure 7 and 8.

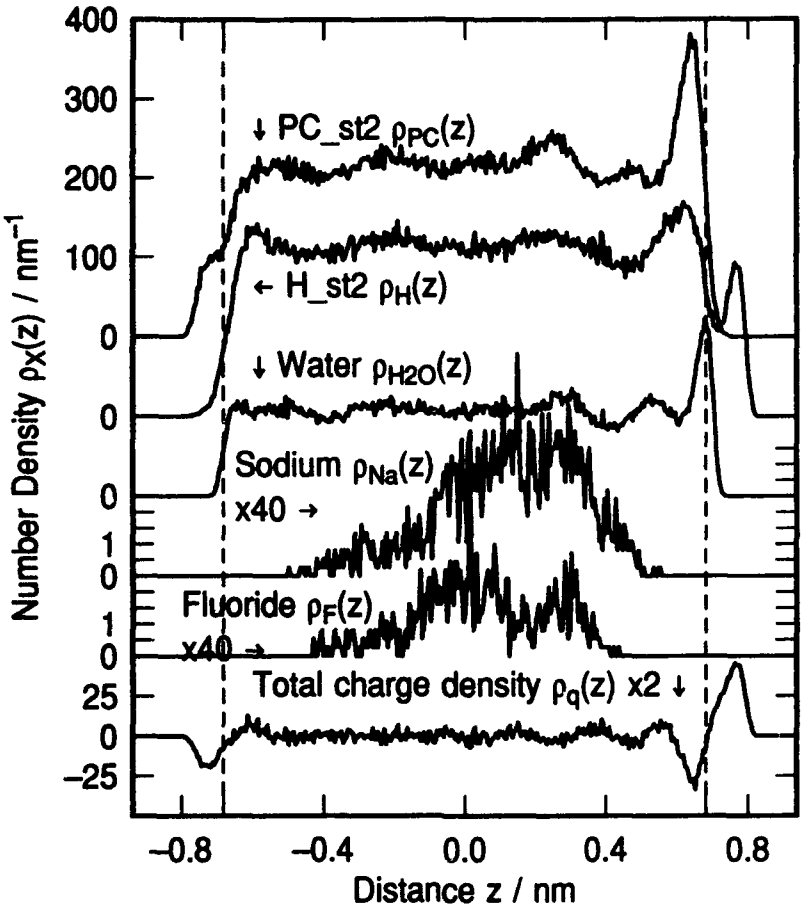

Figure 9. Approximate equivalence interchanged anions and cations, part 1. The charge on the metal was $q_T = q_{im} + q_{uc} = -2$, with $q_{im} = q_{uc} = -1$. Note similarity of water and component density profiles in Figure 7. Density profiles for one fluoride F^-, two sodium ions Na^+ and 155 ST2 water molecules between a charged metal electrode and a dielectric boundary. Image plane at z = 0.931 nm . Repulsive portion of the wall potentials begin at |z| = 0.682 nm.

Figure 10 displays the profiles for two fluoride F^-, one sodium ions Na^+ and 155 ST2 water molecules The charge on the metal was now positive $q_T = q_{im} + q_{uc} = 2$, with $q_{im} = q_{uc} = +1$. Note similarity of water and component density profiles in Figure 7. Note also that the density profiles for Na and F in Figures 9 and 10 when interchanged are almost the same. These calculation extend to mixed electrolytes the conclusion reached in the last section that the water structure in the inner layer is the result of surface electric fields.

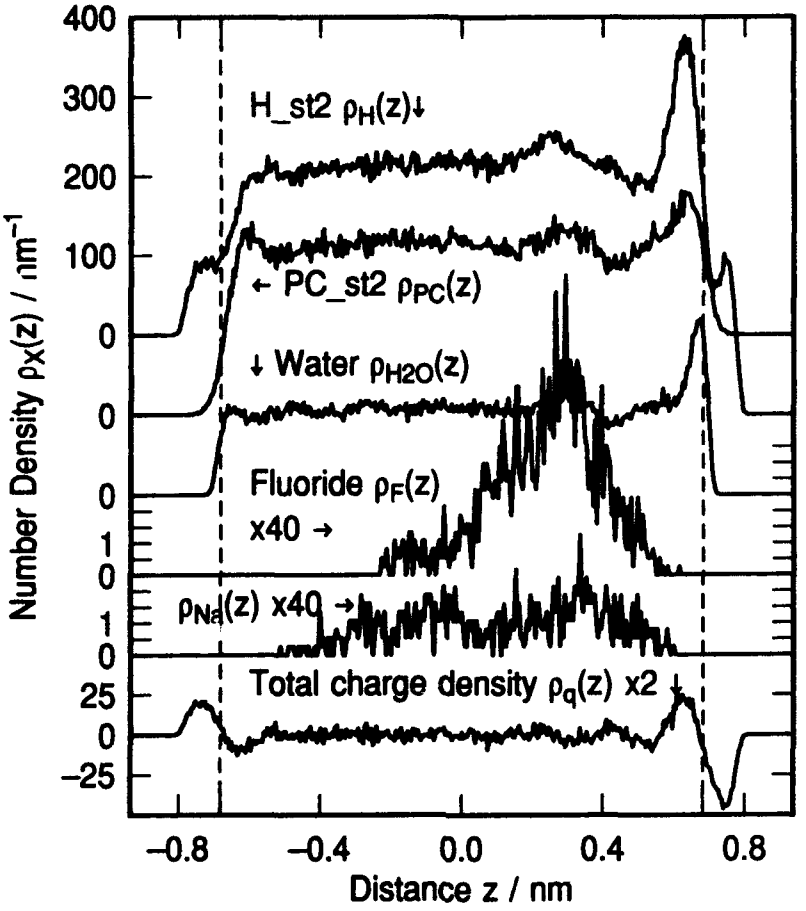

Figure 10. Approximate equivalence interchanged anions and cations, part 2. Note similarity of water and component density profiles in Figure 7. The charge on the metal was positive $q_T = q_{im} + q_{uc} = 2$, with $q_{im} = q_{uc} = +1$. Density profiles for two fluoride F^-, one sodium ions Na^+ and 155 ST2 water molecules between a charged metal electrode and a dielectric boundary. Image plane at z = 0.931 nm . Repulsive portion of the wall potentials begin at |z| = 0.682 nm.

SMALL CATION COADSORBED WITH IODIDE IONS.

In this set of simulations we explore another important aspect of adsorption on metal electrodes, namely the ability of strong contact adsorbers like iodide ions I^- to adsorb on positively charged electrodes in sufficient excess to change the sign of the charge at the interface as observed by an ion in the diffuse layer. In this case cations are attracted out of the diffuse layer region to compensate the excess negative ion charge at the interface. The lithium ion was chosen as cation. We have performed these calculations without and with uncompensated charge.

In the first case the charge on the metal was $q_T = q_{im} = +1$, and in the second case $q_T = q_{im} + q_{uc} = 2$. Figure 11 displays the density profiles for all components of the system and the microscopic charge density. The simulation time was 1000 ps with the first 100 ps discarded for equilibration, and then configurations were stored every 1.0 ps.

Note that both iodide ions adsorbed in one sharply peaked distribution mostly inside the onset of the repulsive wall region, but with a small tail out to smaller z positions. The iodide distribution in zero field is characteristically different from the case when an attractive field exists there being a longer tail into the electrolyte indicating a more weakly bound state. The single Li ion occupies a (possibly weakly bimodal) diffuse-like distribution between -0.6 nm and 0.6 nm. The water profiles hint that the inner surface electric field across the first water layer is weak because the iodide charge is so close to the metal, i.e., the waters are outside the main part of the capacitor is this model. Additionally the large size of the iodides tends to exclude some water from the surface.

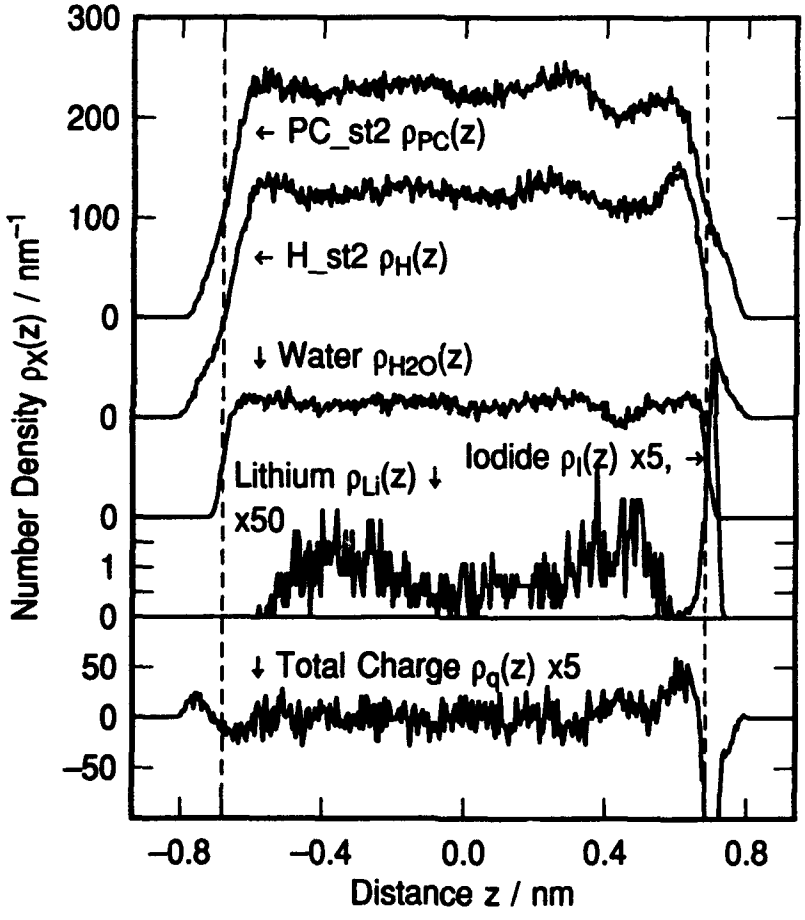

Figure 11. Coadsorption of ions. The charge on the metal was $q_T = q_{im} = +1$. Interface becomes effectively negatively charged after the adsorption of two iodide ions, thereby attracting the positive Li ion. Density profiles for two I^-, one lithium cation Li^+ and 155 ST2 water molecules using the immersed electrode model.

In the second case the charge on the metal was $q_T = q_{im} + q_{uc} = +2$ due to the presence of the extra charge $q_{uc} = +1$. The net charge on the electrode repells the lithium ion. Figure 12 displays the density profiles for all components of the system and the charge density. The simulation time was 1000 ps with the first 100 ps discarded for equilibration, configurations were stored every 0.5 ps. Note that both iodide ions were adsorbed in a sharply

peaked distribution that resembles the single adsorbed iodide distribution calculated by Glosli and Philpott[16]. The single Li ion occupies diffuse-like distribution between -0.6 nm and 0.3 nm and peaks around -0.1 nm. The region between 0.0 and 0.3 nm defines a region of reduced probability of penetrating into inner layer and contacting either the wall or the adsorbed iodide ions.

It is noticeable that the water structure near the metal surface though less well defined than in the case of adsorbed fluoride (see Figures 7, 8 or 10) shows more structure than in Figure 11. Overall the structure resembles water in the field of a positively charged electrode as shown in Figure 5. Some artifacts are expected due to some surface PC reaching the high field region between the iodide layer and the metal.

A final word of caution. The statistics for lithium ions in the simulations described in this section are not as good as in previous calculations. The presence of two iodides on the surface creates a rough surface and the calculations should be run several nanoseconds to permit the positive ion to explore all configuration space.

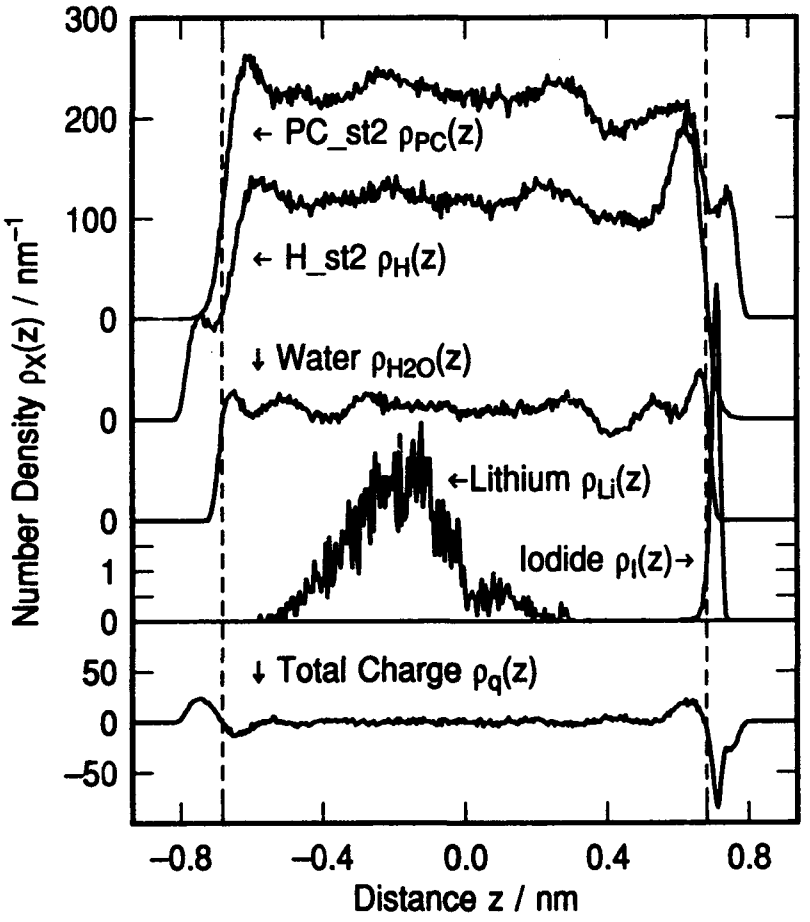

Figure 12. Coadsorption of ions continued. Density profiles for two I^-, one Li^+ and 155 ST2 water molecules next to immersed electrode. The charge on the metal was $q_T = q_{Im} + q_{mc} = +2$.

CONCLUSIONS

In this paper we have shown how a simple model suffices to mimic many phenomena familiar from experiments on electric double layers at the electrolyte-metal interface. There was emphasis on electrostatic interactions and understanding the role played by the inner surface field in driving structural changes in the surface water layer. This is expected to be important for all polar systems. A key element of the calculations was the use of the fast multipole method to accurately and efficiently calculate coulomb interactions so that macroscopic electric fields were computed correctly. Among the phenomena studied were: an oriented boundary layer of water at the electrode when it is charged, penetration of nominally diffuse layer species like hydrated fluoride into the inner layer, and attraction of cations to a positively charged electrode induced by contact adsorption of large ions like iodide.

Finally we point out that the techniques described in this report with minor modifications can be extended to more complex systems, for example: microelectrodes, polymer coated electrodes, biological membranes, globular protein surfaces, and clay surfaces.

ACKNOWLEDGEMENTS

This research was supported in part by the Office of Naval Research.

REFERENCES

1 H. L. von Helmholtz, Ann. Physik **89**, 211 (1853).

2 G. Gouy, Ann. chim. phys. **8**, 291 (1906).

3 G. Gouy, J. Physique **9**, 457 (1910).

4 G. Gouy, Ann. phys. **7**, 129 (1917).

5 D. L. Chapman, Phil. Mag. **25**, 508 (1913).

6 P. Debye and E. Hückel, Physik. Z. **24**, 185 (1923).

7 L. Greengard and V. Rokhlin, J. Comp. Phys. **73**, 325-348 (1987).

8 L. F. Greengard, *The Rapid Evaluation of Potential Fields in Particle Systems*. (The MIT Press, Cambridge, Massachusetts, 1987).

9 J. Carrier, L. Greengard, and V. Rokhlin, Siam J. Sci. Stat. Comput. **9**, 669 (1988).

10 L. Greengard and V. Rokhlin, Chemica Scripta **29A**, 139-144 (1989).

11 R. B. Gennis, *Biomembranes. Molecular Structure and Function.* (Springer-Verlag, New York, 1989), pp. 235-269.

12 H. van Olphen, *Clay Colloid Chemistry* (Kreiger, Malabar Florida, 1991).

13 J. N. Glosli and M. R. Philpott, J. Chem. Phys. **96**, 6962-6969 (1992).

14 J. N. Glosli and M. R. Philpott, J. Chem. Phys. **98**, 9995-10008 (1993).

15 J. N. Glosli and M. R. Philpott, Electrochem. Soc. Symposium Proc. **93-5**, 80-90 (1993).

16 J. N. Glosli and M. R. Philpott, Electrochem. Soc. Symposium Proc. **93-5**, 90-103 (1993).

17 J. O. Bockris and A. K. Reddy, *Modern Electrochemistry, Vol.1* (Plenum Press, New York, 1973).

18 J. O. Bockris and A. K. Reddy, *Modern Electrochemistry, Vol.2* (Plenum Press, New York, 1973).

19 C. Y. Lee, J. A. McCammon, and P. J. Rossky, J. Chem. Phys. **80**, 4448-4455 (1984).

20 J. P. Valleau and A. A. Gardner, J. Chem. Phys. **86**, 4162-4170 (1987).

21 Y. J. Rhee, J. W. Halley, J. Hautman, and A. Rahman, Phys. Rev. B **40**, 36-42 (1989).

22 A. M. Brodsky, M. Watanabe, and W. P. Reinhardt, Electrochimica Acta **36**, 1695-1697 (1991).

23 M. Watanabe, A. M. Brodsky, and W. P. Reinhardt, J. Phys. Chem. **95**, 4593 (1991).

24 N. Parsonage and D. Nicholson, J. Chem. Soc. Faraday Trans. 2 **82**, 1521-1535 (1986).

25 N. Parsonage and D. Nicholson, J. Chem. Soc. Faraday Trans. 2 **83**, 663 - 673 (1987).

26 A. A. Gardner and J. P. Valleau, J. Chem. Phys. **86**, 4171-4176 (1987).

27 E. Spohr and K. Heinzinger, Electrochimica Acta **33**, 1211-1222 (1988).

28 E. Spohr and K. Heinzinger, Ber. Bunsenges. Phys. Chem. **92**, 1358-1363 (1988).

29 K. Heinzinger and E. Spohr, Electrochimica Acta **34**, 1849-1856 (1989).

30 J. Hautman, J. W. Halley, and Y. Rhee, J. Chem. Phys. **91**, 467-472 (1989).

31 K. Foster, K. Raghavan, and M. Berkowitz, Chem. Phys. Lett. **162**, 32-388 (1989).

32 K. Raghavan, K. Foster, K. Motakabbir, and M. Berkowitz, J. Chem. Phys. **94**, 2110-2117 (1991).

33 R. Kjellander and S. Marcelja, Chemica Scripta **25**, 73-80 (1985).

34 E. Spohr and K. Heinzinger, J. Chem. Phys. **84**, 2304-2309 (1986).

35 J. Seitz-Beywl, M. Poxleitner, and K. Heinzinger, Z. Naturforsch. **46A**, 876 (1991).

36 D. A. Rose and I. Benjamin, J. Chem. Phys. **95**, 6856-6865 (1991).

37 K. Heinzinger, Pure Appl. Chem. **63**, 1733-1742 (1991).

38 G. E. Schacher and F. W. de Wette, Phys. Rev. **136A**, 78-91 (1965).

39 D. C. Grahame., Chem. Rev. **41**, 441 (1947).

40 D. C. Grahame., J. Amer. Chem. Soc. **79**, 2093 (1957).

41 G. Lippmann, Ann. Chim. Phys. (Paris) **5**, 494 (1875).

42 H. D. Hurawitz, J. Electroanal. Chem. **10**, 35 (1965).

43 E. Dutkiewicz and R. Parsons, J. Electroanal. Chem. **11**, 100 (1966).

44 F. C. Anson, Accts Chem. Res. **8**, 400-407 (1975).

45 R. Parsons, Chem. Rev. **90**, 813-826 (1990).

46 A. T. Hubbard, Chem. Rev. **88**, 633 - 656 (1988).

47 J. O. Bockris and A. Gonzalez-Martin, *Spectroscopic and Diffraction Techniques in Interfacial Electrochemistry, NATO ASI Series C* (Kluwer,Dordrecht,Holland, 1990), pp. 1-54.

48 J. W. Albery, *Electrode Kinetics* (Clarendon Press, Oxford, 1975).

49 L. Antropov, *Theoretical Electrochemistry* (Mir Publishers, Moscow, 1972).

50 J. O. Bockris and S. U. Khan, *Quantum Electrochemistry* (Plenum Press, New York, 1979).

51 J. W. Halley, B. Johnson, D. Price, and M. Schwalm, Phys. Rev. B **31 B**, 7695-7709 (1985).

52 J. W. Halley, Supperlattices and Microstructures **2**, 165-172 (1986).

53 J. W. Halley and D. Price, Phys. Rev. B **35 B**, 9095-9102 (1987).

54 W. Schmickler and D. Henderson, Prog. Surf. Sci. **22**, 323 (1986).

55 D. Henderson, *Trends in Interfacial Electrochemistry* (Reidel, Dordrecht, Holland, 1986), p. 183.

56 O. R. Melroy, M. G. Samant, G. L. Borges, J. G. Gordon, L. Blum, J. H. White, M. J. Albarelli, M. McMillan, and H. D. Abruna, Langmuir **4**, 728 (1988).

57 M. F. Toney, J. G. Gordon, and O. R. Melroy, SPIE Proceedings **1550**, 140 (1991).

58 M. F. Toney, J. N. Howard, J. Richer, G. L. Borges, J. G. Gordon, O. R. Melroy, D. G. Wiesler, D. Yee, and L. B. Sorensen, Nature (1994).

59 T. Tadjeddine, D. Guay, M. Ladouceur, and G. Tourillon, Phys. Rev. Lett. **66**, 2235 - 2238 (1991).

60 F. H. Stillinger and A. Rahman, J. Chem. Phys. **60**, 1545 (1974).

61 O. Steinhauser, Mol. Phys. **45**, 335-348 (1982).

[62] K. Heinzinger, *Computer Modelling of Fluids Polymers and Solids*, (Kluwer,Dordrecht, 1990), pp. 357-404.

[63] M. P. Allen and D. J. Tildesley, *Computer Simulation of Liquids* (Oxford University Press, Oxford, 1989), pp. 88-90.

[64] D. J. Evans, Mol. Phys. **34**, 317-325 (1977).

[65] D. J. Evans and S. Murad, Mol. Phys. **34**, 327-331 (1977).